17

Fronts, Jets, and Vortices

Summary: When the Rossby number is not small, the dynamics are nonlinear and non-quasi-geostrophic. Such regimes exhibit fronts and jets, the latter being related to the former via pressure gradients. Strong jets meander and shed vortices, which also populate this dynamical regime. The chapter ends with a brief discussion of geostrophic turbulence, the state of many interacting vortices under the influence of Coriolis effects.

17-1 FRONTS AND JETS

17-1-1 Origin and Scales

A common occurrence in the atmosphere and ocean is the encounter of two fluid masses that, due to separate origins, have distinct properties. The result is the existence of a local transitional region that is relatively narrow (compared to the dimensions of the main fluid masses) and where properties vary spatially much more rapidly than on either side. Such a region of intensified gradients of fluid properties is called a *front.*

Typically, the adjacent fluid masses have different densities, and the front is accompanied by a relatively large pressure gradient. Under the action of Coriolis forces,

the process of geostrophic adjustment is at work, leading to a relatively intense flow aligned with the front. The much weaker density gradients in the main part of each fluid mass confine the motion to the frontal region, and the flow exhibits the form of a jet. The most notable jet in the atmosphere is the so-called polar-front jet stream found around a latitude of 45°N and a few kilometers above sea level (pressure around 300 millibars), at the boundary between subtropical and polar air masses (Figure 17-1). In

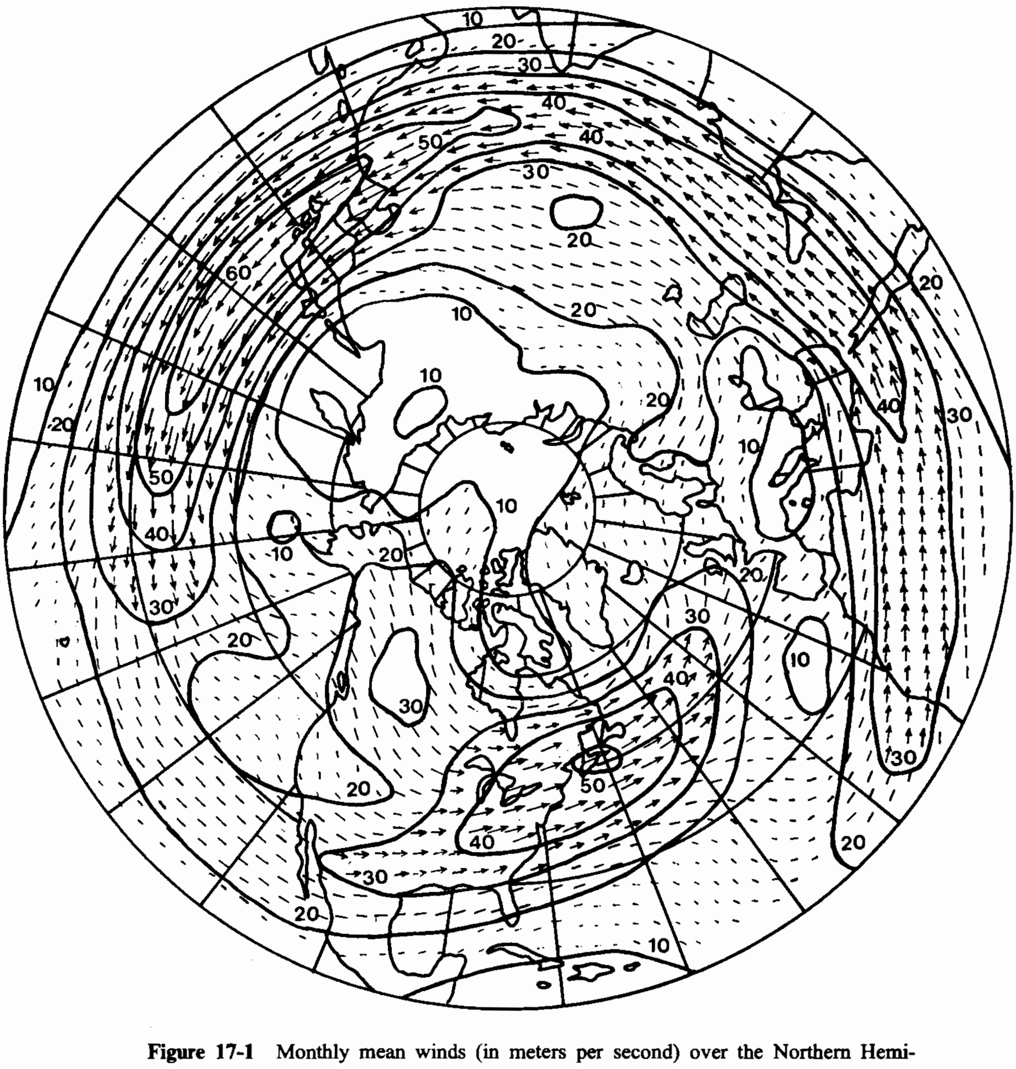

Figure 17-1 Monthly mean winds (in meters per second) over the Northern Hemisphere for January 1991 at the 300-mb pressure level. Note the jet stream around the 45°N parallel, except over the eastern North Pacific and eastern North Atlantic, where blockings are present. (From National Weather Service, NOAA, Department of Commerce, Washington, D.C.)

the ocean, a surface-to-bottom front is often found in the vicinity of the shelf break owing to different water properties above the continental shelf and in the deep ocean; such a front is invariably accompanied by currents along the shelf (Figure 17-2).

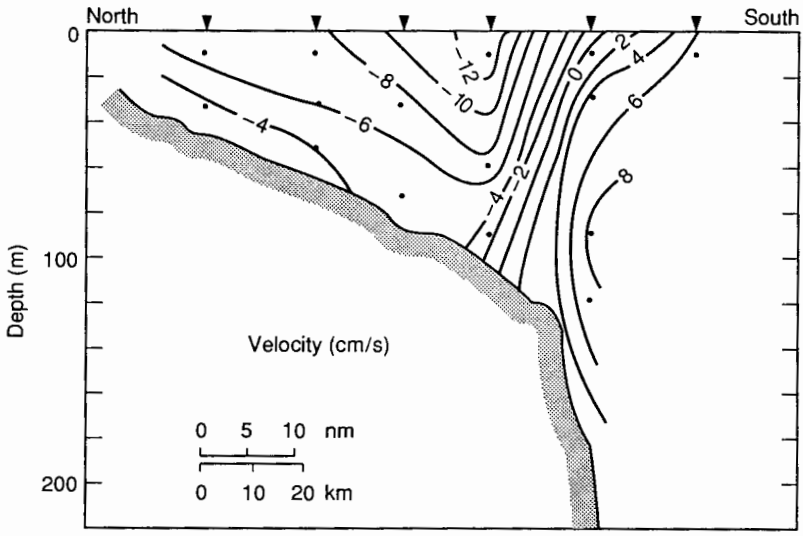

Figure 17-2 Monthly mean along shelf currents for April 1979 across the shelf break on the southern flank of Georges Bank (41°N, 67°W). The units are centimeters per second. Positive values indicate flow pointing into the page. (From Beardsley et al., 1983, as adapted by Gawarkiewicz and Chapman, 1992.)

According to Section 13-1, the simultaneous presence of a horizontal gradient of density and a vertical gradient of horizontal velocity can yield a thermal-wind balance, which may persist for quite some time. Our discussions of geostrophic adjustment (Section 13-2) demonstrated how such a balance can be achieved following the penetration of one fluid mass into another of different density and indicated that the width of the transitional region is measured by the internal radius of deformation, expressed as

$$R = \frac{NH}{f} \sim \frac{\sqrt{g'H}}{f} \tag{17-1}$$

in the respective cases of continuous stratification and layered configuration. Here f is the Coriolis parameter, H is an appropriate height scale, N is the stratification frequency, and g' is a suitable reduced gravity. If the density difference between the fluid masses is $\Delta\rho$, the accompanying pressure difference is $\Delta P \sim \Delta\rho\ gH = \rho_0 g'H$, and, via geostrophy, the velocity scale is

$$U = \frac{\Delta P}{\rho_0 f R} \sim \frac{g'H}{fR} = \sqrt{g'H}\,. \tag{17-2}$$

The Froude and Rossby numbers are, respectively,

$$Fr = \frac{U}{NH} \sim \frac{\sqrt{g'H}}{fR} \sim 1, \tag{17-3}$$

$$Ro = \frac{U}{fR} \sim \frac{\sqrt{g'H}}{fR} \sim 1, \tag{17-4}$$

and thus both are on the order of unity, implying that the effects of stratification and rotation are equally important within the jet.

The jet has a velocity maximum, coinciding more or less with the location of the maximum density gradient, on both sides of which the velocity decays. The corresponding shears form a distribution of relative vorticity that is clockwise on the right and counterclockwise on the left (respectively, anticyclonic and cyclonic in the Northern Hemisphere). This shear vorticity scales as $Z = U/R \sim f$ and is thus comparable to the planetary vorticity.

17-1-2 Meanders

Observations reveal that all jets meander, unless they are strongly constrained by the local geography. As a fluid parcel flows in a meander, its path curves, subjecting it to a transverse centrifugal force on the order of KU^2, where K is the local curvature of the trajectory (the inverse of the radius of curvature). This force can be met by a reduction or increase of the Coriolis force if the parcel's velocity adjusts by ΔU, such that $f\Delta U \sim KU^2$, or

$$\frac{\Delta U}{U} \sim \frac{KU}{f} \sim KR. \tag{17-5}$$

In the Northern Hemisphere ($f > 0$), the Coriolis force acts to the right of the fluid parcel, and thus a rightward turn causing a centrifugal force to the left necessitates a greater Coriolis force and an acceleration ($\Delta U > 0$). Similarly, a leftward turn is accompanied by a jet deceleration ($\Delta U < 0$). The reverse conclusions hold for the Southern Hemisphere, but in all cases, the stronger the curvature, the larger the change in velocity, according to (17-5).

The same result can be obtained by considering the changes in relative vorticity. Neglecting the beta effect and eventual vertical stretching or squeezing, the relative vorticity is conserved. It can be expressed locally as

$$\zeta = \frac{\partial v}{\partial x} - \frac{\partial u}{\partial y} = \frac{\partial V}{\partial n} - KV,$$

where $V = (u^2 + v^2)^{1/2}$ is the flow speed (scaling as U), n the cross-jet coordinate (measured positively to the right of the local velocity and scaling as R), and K the jet curvature (positive clockwise). The first term, $\partial V/\partial n$, is the contribution of the shear and the second, $-KV$, represents a vorticity due to the turning of the flow path. We

shall call these contributions shear vorticity and orbital vorticity, respectively. In a rightward turn ($K > 0$), the fluid parcel acquires clockwise orbital vorticity, on the order of KU, which must be at the expense of shear vorticity, $\Delta U/R$. Equating KU to $\Delta U/R$ again leads to (17-5).

The change in shear vorticity implies a shift of the parcel with respect to the jet axis. To show this, let us take, for example, the fluid parcel that possesses the maximum velocity (i.e., it is on the jet axis) upstream of the meander; there it has no shear and no orbital vorticity. If this parcel turns to the right in the meander, it acquires clockwise orbital vorticity, which is compensated by a counterclockwise shear vorticity of the same magnitude. Thus, the parcel must now be on the left flank of the jet. The parcel occupying the jet axis (having maximum velocity and thus no shear vorticity) is one that was on the right flank of the jet upstream and has exchanged its entire clockwise shear vorticity for an equal clockwise orbital vorticity. From this, it is straightforward to conclude that all parcels are displaced leftward with respect to the jet axis in a rightward meander, and vice versa. (This rule is easy to remember: Fluid parcels shift across the jet in the direction of the centrifugal force.)

A consequence of these vorticity adjustments created by meandering is that fluid parcels near the edges may separate from the jet or be captured by it. Indeed, a parcel relatively distant from the jet axis may have such low vorticity that it cannot trade shear vorticity for orbital vorticity (Figure 17-3).

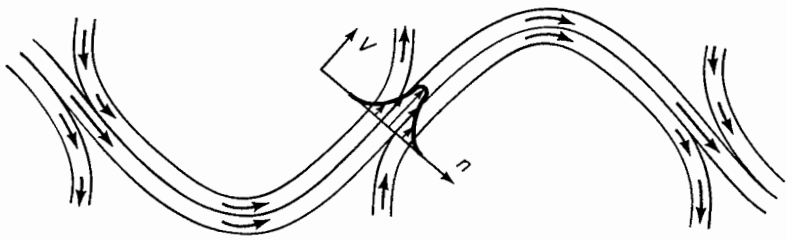

Figure 17-3 Separation and capture of fluid parcels along the edges of a meandering jet. This situation occurs because the vorticity adjustments required by the meanders force marginal parcels to reverse their velocity.

The preceding considerations ignored the beta effect, by which the Coriolis force is able to vary. Let us limit ourselves here to the case of an eastward (i.e., westerly) jet in the Northern Hemisphere, which is the case of the atmospheric jet stream and the Gulf Stream in the North Atlantic beyond Cape Hatteras. In a northern meander excursion, called a *crest* (because it appears higher on a map), the curvature is rightward or anticyclonic (Figure 17-4). The meridional displacement Y, the meander's amplitude, causes an augmentation to the Coriolis force on the order of $\beta_0 YU$, acting to the right of the parcel. On the other hand, the centrifugal force on the order of KU^2 acts to its left. Three cases are possible: $\beta_0 Y$ is much less than, on the order of, or much greater than KU.

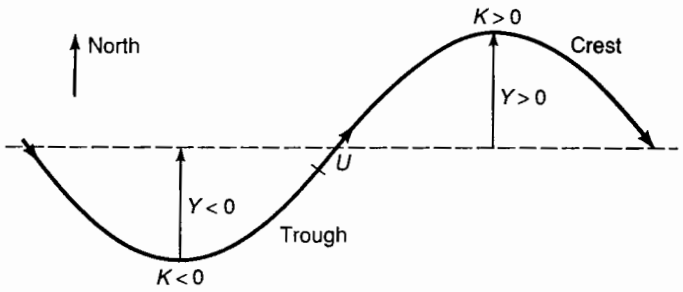

Figure 17-4 Meandering of an eastward jet on the beta plane (Northern Hemisphere). If the meridional displacement Y and the curvature K are related by $\beta_0 Y \sim KU$, changes in planetary and orbital vortices are comparable and opposite in sign, leaving the velocity profile of the jet (shear vorticity) relatively unperturbed.

If $\beta_0 Y$ is much less than KU, the beta affect mitigates the curvature effect, but the conclusions derived before remain qualitatively unchanged. This is the case of weak meander amplitudes (small Y) and/or short meander wavelengths (large K).

If $\beta_0 Y$ is on the order of KU, then the beta and curvature effects can balance each other, leaving the structure of the jet barely affected. Considering sinusoidal meanders $Y(x) = A \sin lx$, where A is the meander amplitude, $\lambda = 2\pi/l$ is its wavelength, and x is the eastward coordinate, we deduce that at the meander's peak ($\sin lx = +1$), the meridional displacement Y is A and the curvature $K = -[d^2Y/dx^2]/[1 + (dY/dx)^2]^{3/2}$ is l^2A. The balance $\beta_0 Y \sim KU$ then yields $\beta_0 \sim l^2 U$, or

$$\lambda = \frac{2\pi}{l} = 2\pi \sqrt{\frac{U}{\beta_0}}.$$

From this emerges a particular length scale,

$$L = \sqrt{\frac{U}{\beta_0}}, \tag{17-6}$$

which we shall call the *critical meander scale*. Cressman (1948) noted its importance in relation to the development of long waves on the atmospheric jet stream, whereas Moore (1963) obtained a solution to an ocean-circulation model that exhibits meanders at that scale. Later, Rhines (1975) demonstrated how this same scale plays a pivotal role in the evolution of geostrophic turbulence on the beta plane.

In very large meanders, where meridional displacements are large and curvatures are small ($\beta_0 Y \gg KU$), the beta effect dwarfs the curvature effect, and the trade-off is almost exclusively between changes in planetary vorticity and shear vorticity. In a meander crest (greater f), the shear vorticity must become less cyclonic or more anticyclonic.

Meanders on a jet do not remain stationary but propagate, usually downstream and rarely upstream. The direction of propagation can be inferred from vorticity consider-

ations, as outlined previously. In the absence of the beta effect (or $\beta_0 Y \ll KU$), leftward and rightward turns create, respectively, clockwise and counterclockwise shear vorticity. Picturing these vorticity anomalies as vortices at the meanders' tips (Figure 17-5a), we infer that the entrainment velocities at the inflection points between meanders all have a downstream component and that the meander pattern translates downstream. On a westerly jet, this direction is eastward. At the opposite extreme of a large beta effect and negligible curvature ($\beta_0 Y \gg KU$), the vorticity anomalies are cyclonic in troughs and anticyclonic in crests (Figure 17-5b). The entrainment velocities at the inflection points all point westward. On a westerly jet, this is upstream. This mechanism is the same as that invoked in Section 6-6 to explain the westward phase propagation of planetary waves. (Compare Figure 17-5b with Figure 6-7.)

We note, therefore, that curvature and beta effects induce opposite meander-propagation tendencies on an eastward jet. Comparing $\beta_0 Y$ with KU—or, equivalently, the wavelength to the critical meander scale—we conclude that if the former is larger than the latter, the meander propagates upstream (westward), and in the opposite direction otherwise. The meander is stationary if the tendencies cancel each other, which occurs if its wavelength is near the critical meander scale. Since this scale is rather long (220 km in the ocean and 1600 km in the atmosphere, with $\beta_0 = 2 \times 10^{-11}$ $m^{-1} \cdot s^{-1}$

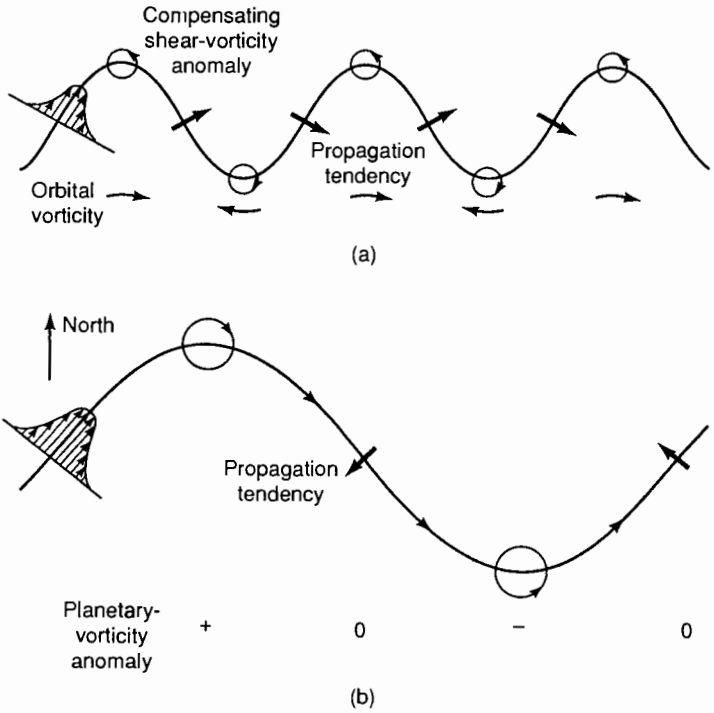

Figure 17-5 Schematic descriptions explaining why (a) curvature and (b) beta effects on an eastward jet induce meander-propagation tendencies that are, respectively, downstream and upstream.

and U equal to 1 m/s and 50 m/s, respectively), observed meanders are usually of the curvature-type and propagate eastward.

17-1-3 Multiple Equilibria

Because the critical meander scale depends on the jet speed U and also because the relation $\beta_0 Y \sim KU$ depends on the shape of the meander (Y and K are not simply related if the meander is other than sinusoidal), the critical size for meander stationarity depends on the jet speed and the meander shape. This conclusion is the basis of one explanation for the bimodality of the Kuroshio (Figure 17-6). The geography of coastal Japan and the regional bottom topography force this intense current of the western North Pacific to pass through two channels, south of Yakushima Island (30°N, 134°E) and between Miyake and Hachijo Islands near the Izu Ridge (34°N, 140°E). Between these two points, the current is known to assume one of two preferential states: a relatively straight path or a curved path with a substantial southward excursion. Each pattern persists for several years, whereas the transition from one to the other is relatively brief. The theory (Robinson and Taft, 1972; Masuda, 1982) explains this bimodal character by arguing that a stationary meander with a half-wavelength meeting the geographical specification may or may not exist, depending on the jet velocity. Calculations show that the meander-state occurs if the jet velocity does not exceed a certain threshold value. At any velocity below this value, there exists a stationary-meander shape that meets the geographical constraints. At larger velocities, no stationary meander is possible, and the jet must assume a straight path.

The atmospheric analogue of this oceanic situation is known as *blocking*, a word now used in a sense different from that used in Chapter 9. Here, blocking is a midlatitude phenomenon characterized by the unusual persistence of a nearly stationary meander on an eastward jet over topographic irregularities (Figure 17-1). The theory (Charney and DeVore, 1979; Charney and Flierl, 1981) again invokes multiplicity of equilibrium solutions, including the normal state (no meander) and the anomalous blocking configuration (with large meander).

17-1-4 Stretching and Topographic Effects

Up to here, our considerations of vorticity adjustments in a jet meander included exchanges among planetary, shear, and orbital vorticity, for an unchanged total. This is correct only for barotropic jets, whereas in a baroclinic jet, in which vertical stretching can occur, potential vorticity rather than vorticity is the conserved quantity.

A complete theory involving all relevant dynamics such as momentum and mass balances is beyond our scope, and we will derive here only the vertical-stretching tendency experienced by a fluid parcel in a meander. Assuming that the trade-off is solely between orbital vorticity due to the meander's curvature and vertical stretching, we reason that a meander crest (with anticyclonic orbital vorticity) lowers the total vorticity and thus calls for a proportional decrease in the column's vertical thickness. If, furthermore, the layer thickness varies like pressure (as for the one-layer reduced-

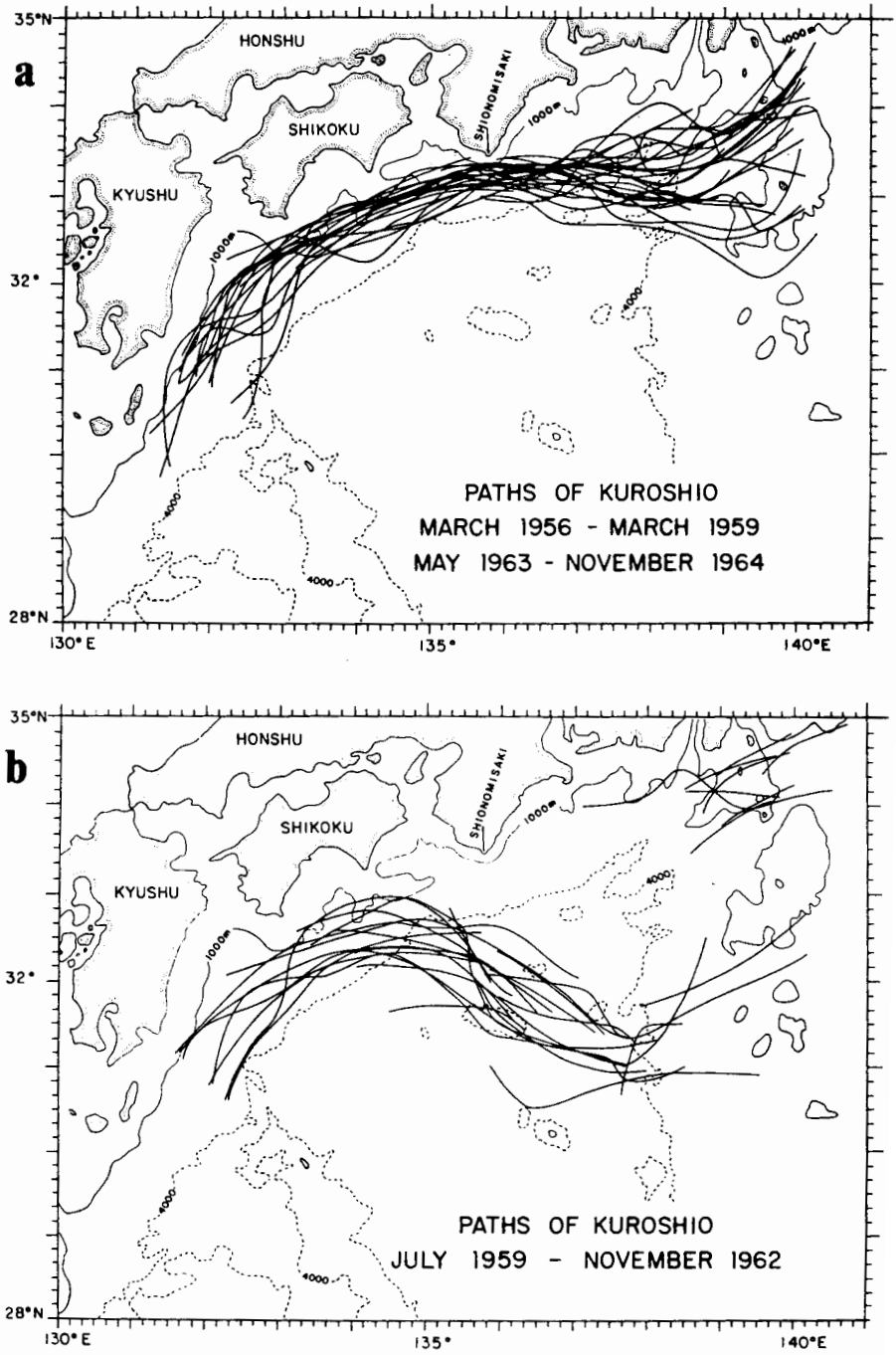

Figure 17-6 Observed Kuroshio paths: (a) straight jet and (b) stationary meander. (From Robinson and Taft, 1972).

gravity system where the pressure is given by $p = \rho_0 g' h$), vertical squeezing translates into a lower pressure and, by geostrophy, into a shift toward the cyclonic side of the jet (left in the Northern Hemisphere). In meander troughs, fluid columns are vertically stretched and shifted toward the anticyclonic side of the jet. In an oceanic surface jet such as the Gulf Stream, such a modification causes upwelling upon approaching crests and downwelling upon approaching troughs. Observations (Bower and Rossby, 1989) reveal such behavior.

Just as meanders generate vertical stretching or squeezing, vertical stretching or squeezing induced by topography can cause meanders. To illustrate this, let us consider the case of a zonal jet (barotropic or baroclinic) on the beta plane that encounters a topographic step (Figure 17-7). If the jet is flowing eastward (the usual situation) and

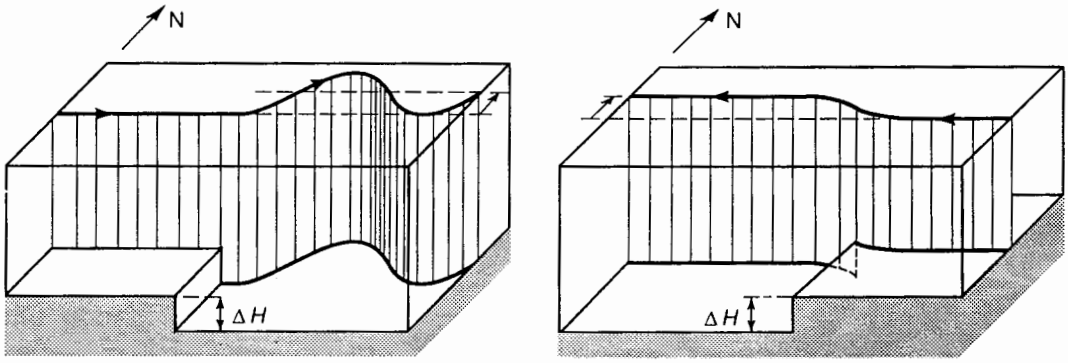

Figure 17-7 Eastward and westward jets over a topographic step: (a) the eastward jet develops an oscillatory behavior downstream of the step, whereas (b) the westward jet feels the influence of the step upstream and executes a single meander. Both experience a net meridional shift.

enters a deeper region, the expansion in layer thickness translates first into a cyclonic deflection, away from the equator. As the Coriolis parameter increases away from the equator, this cyclonic vorticity is progressively exchanged downstream by a greater planetary vorticity, and the jet curvature weakens. Further poleward progression reverses the sense of orbital vorticity, and the jet oscillates back and forth about a new latitude (Figure 17-7a). The average northward shift, Y, of the jet axis corresponds to an exchange between vertical stretching and increased planetary vorticity:

$$\frac{\beta_0 Y}{f_0} \sim \frac{\Delta H}{h}, \tag{17-7}$$

where ΔH is the height of the topographic step and h is the upstream thickness of the jet. Because the first meander is rooted at the location of the step, the meander must be stationary, and the wavelength is comparable to the critical meander scale.

The same argument can be invoked for an eastward jet entering a shallower region to conclude that the flow exhibits a stationary oscillation about a net equatorward shift, given by (17-7) where ΔH is now negative. However, the argument fails for westward jets. Upon entering a deeper region, a fluid parcel acquires cyclonic vorticity and turns equatorward, its planetary vorticity decreases, further increasing the orbital vorticity. Clearly, if this were the case, the jet would be looping onto itself. Instead, the jet begins to be distorted upstream of the topographic step (Figure 17-7b), acquiring a cyclonic curvature in which the increasing orbital vorticity is compensated by a decrease in planetary vorticity. The jet thus reaches the step at an oblique angle. The nature of the vorticity adjustments past the step progressively restores the jet's original zonal orientation. A remaining meridional shift remains, expressing a balance between changes in planetary vorticity and vertical thickness. The reader can verify that this shift is again given by (17-7).

17-1-5 Instabilities

In addition to their propagation, meanders on a jet also distort and frequently grow, close onto themselves, and form eddies that separate from the rest of the jet. Such a finite change to the jet structure results from an instability, the nature of which is barotropic (Chapter 7), baroclinic (Chapter 16), or mixed. Barotropic instability proceeds with the extraction of kinetic energy from the horizontally sheared flow to feed the growing meander. The greater the shear in the jet, the more likely is this type of instability. Baroclinic instability, on the other hand, is associated with a conversion of available potential energy from the horizontal density distribution in balance with the thermal wind. Whereas the example treated in Section 7-4 suggests that critical wavelengths associated with barotropic instability scale as the jet width, consideration of baroclinic instabilitity points to the critical role of the internal radius of deformation [see equation (16-15)]. If the two length scales are comparable, as is the case in a baroclinic jet with finite Rossby number, both processes may be equally active, and the instability is most likely of the mixed type (Orlanski, 1968; Griffiths et al., 1982; Killworth et al., 1984). The beta effect further complicates the situation, occasionally facilitating the eddy detachment process: The large meridional displacement of the growing meander induces a westward-propagation tendency, whereas the high-curvature regions where the meander attaches to the rest of the jet induce a downstream propagation tendency. The result is a complex situation in which the outcome sensitively dependent on the relative magnitudes of the different effects (Flierl et al., 1987; Robinson et al., 1988). The meandering and eddy shedding of the Gulf Stream manifest this complexity.

The development of synoptic-scale weather disturbances, a process now called *cyclogenesis*, is thought to be initiated mostly by baroclinic instability, whereas accompanying finer-scale processes, such as cold and warm fronts, are explained by nongeostrophic dynamics. The interested reader is referred to the book by Holton (1992).

17-2 VORTICES

A vortex, or eddy, is defined as a closed circulation that is relatively persistent. By persistency, we mean that the turnaround time of a fluid parcel embedded in the structure is shorter than the time during which the structure remains identifiable. A *cyclone* is a vortex where the rotary motion is in the same sense as the earth's rotation, counterclockwise in the Northern Hemisphere and clockwise in the Southern Hemisphere. An *anticyclone* rotates the other way, clockwise in the Northern Hemisphere and counterclockwise in the Southern Hemisphere. The prototypical vortex is a steady circular motion on the f-plane.

Using cylindrical coordinates, we can express the balance of forces in the radial direction r (measured outward) as follows:

$$-\frac{v^2}{r} - fv = -\frac{1}{\rho_0}\frac{\partial p}{\partial r}, \tag{17-8}$$

where v is the orbital velocity (positive counterclockwise) and p is the pressure (or Montgomery potential). Both v and p may be dependent upon the vertical coordinate, either height z or density ρ. This equation, called the *gradient-wind balance*, represents an equilibrium between three forces, the centrifugal force (first term), the Coriolis force (second term), and the pressure force (third term). Although the centrifugal force is always directed outward, the Coriolis and pressure forces can be directed either inward or outward, depending on the direction of the orbital flow and on the center pressure.

If we introduce the following scales, U for the orbital velocity, L for r (measuring the vortex radius), and ΔP for the pressure difference between the ambient value and that at the vortex center, we note that the terms composing (17-8) scale, respectively, as

$$\frac{U^2}{L}, \quad fU, \quad \frac{\Delta P}{\rho_0 L}.$$

At low Rossby numbers ($Ro = U/fL \ll 1$), the first term is negligible relative to the second (i.e., the centrifugal force is small compared to the Coriolis force), the balance is nearly geostrophic, providing

$$fU = \frac{\Delta P}{\rho_0 L},$$

and thus $U = \Delta P/(\rho_0 fL)$. Since the pressure difference is most likely the result of a density anomaly $\Delta\rho$, the hydrostatic balance provides $\Delta P = \Delta\rho gH = \rho_0 g'H$, where H is the appropriate height scale (thickness of vortex) and $g' = g\Delta\rho/\rho_0$ is the reduced gravity. This leads to $U = g'H/fL$ and

$$Ro = \frac{U}{fL} = \frac{g'H}{f^2L^2} = \left(\frac{R}{L}\right)^2,$$

in which we recognize the internal deformation radius $R = (g'H)^{1/2}/f$. Thus, a small Rossby number occurs as a consequence of a horizontal scale large compared to the

deformation radius. This is typically the case in the largest weather cyclones and anticyclones at midlatitudes and in large-scale oceanic gyres (Figure 17-8 top).

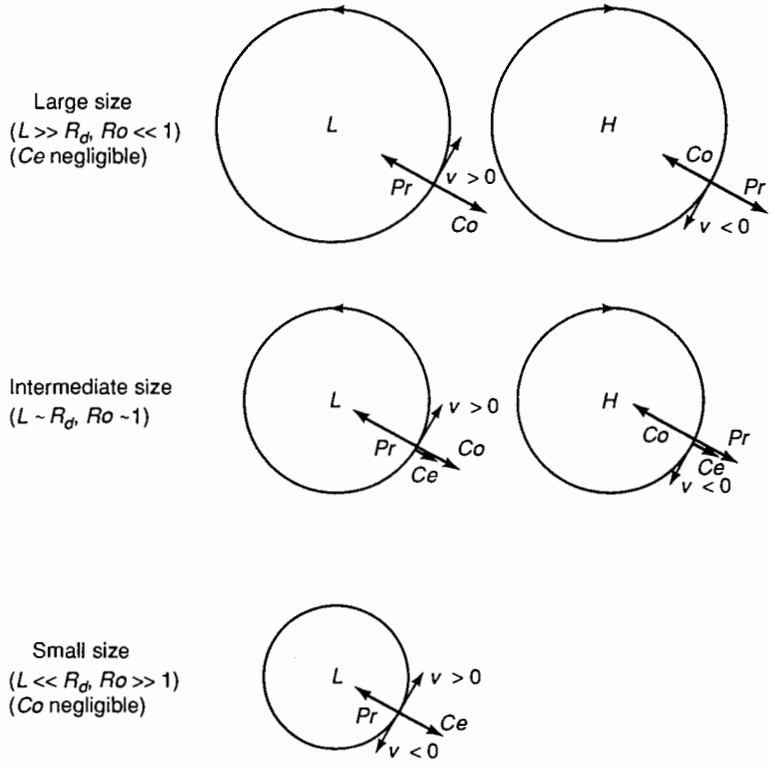

Figure 17-8 Balances between pressure (*Pr*), Coriolis (*Co*), and centrifugal (*Ce*) forces in Northern Hemispheric circular vortices. The letters *L* and *H* indicate low and high pressures, respectively.

At scales on the order of the deformation radius, L can be taken equal to R, the Rossby number is on the order of unity, the velocity scale is $U = (g'H)^{1/2}$, and the centrifugal force is comparable to the Coriolis force. Around a low pressure, the outward centrifugal force partially balances the inward pressure force, leaving the Coriolis force to meet only the difference. By contrast, the Coriolis force acting on the flow around a high pressure must balance both the outward pressure force and the outward centrifugal force (Figure 17-8 middle). Consequently, the orbital velocity in an anticyclone is greater than that in a cyclone of identical size and equivalent pressure anomaly. Tropical hurricanes (Anthes, 1982; Emmanuel, 1991) and the so-called rings shed by the Gulf Stream (Flierl, 1987; Olson, 1991) fall in this category.

At progressively shorter radii, the centrifugal force becomes increasingly important, and the difference between cyclones and anticyclones amplifies. For $L \ll R$, the Coriolis

force becomes negligible. The cyclone-anticyclone nomenclature loses its meaning, and the relevant characteristic is the sign of the pressure anomaly. The inward force around a low pressure is balanced by the outward centrifugal force regardless of the direction of rotation (Figure 17-8 bottom). Such a state is said to be in *cyclostrophic balance.* Examples are tornadoes and bathtub vortices. A vortex with high-pressure center cannot exist, because pressure and centrifugal forces are both directed outward.

It is interesting to determine the minimum size for which an anticyclone of given pressure anomaly can exist. Returning to the gradient-wind balance where we introduce $v = -fr/2 + v'$, we write

$$\frac{f^2 r}{4} + \frac{1}{\rho_0}\frac{\partial p}{\partial r} = \frac{1}{r} v'^2 \geq 0.$$

Integrating over the radius a of the vortex and defining the pressure anomaly $\Delta p = p(r = 0) - p(r = a)$, we then obtain

$$a^2 \geq \frac{8\Delta p}{\rho_0 f^2}. \tag{17-9}$$

For a low-pressure center ($\Delta p < 0$), this inequality yields no constraint, whereas for a high-pressure center ($\Delta p > 0$) it specifies a minimum vortex radius. Below this minimum, high-pressure centers simply do not exist as isolated steady structures.

Let us now examine how an existing vortex can move within the fluid that surrounds it. To do this, we consider a vortex contained within a single layer of fluid, be it the lowest, the uppermost, or any intermediate layer in the fluid. If the local thickness of this layer is h and the pressure (actually, Montgomery potential) is p, we write, in density coordinates,

$$\frac{\partial u}{\partial t} + u\frac{\partial u}{\partial x} + v\frac{\partial u}{\partial y} - fv = -\frac{1}{\rho_0}\frac{\partial p}{\partial x}, \tag{17-10a}$$

$$\frac{\partial v}{\partial t} + u\frac{\partial v}{\partial x} + v\frac{\partial v}{\partial y} + fu = -\frac{1}{\rho_0}\frac{\partial p}{\partial y}, \tag{17-10b}$$

$$\frac{\partial h}{\partial t} + \frac{\partial}{\partial x}(hu) + \frac{\partial}{\partial y}(hv) = 0. \tag{17-10c}$$

We further restrict ourselves to the f-plane. At large distances from the vortex center, in what can be considered the ambient fluid, we assume that there exists a steady uniform flow $(\bar{u}, \bar{v})$ and a uniform thickness gradient $(\partial\bar{h}/\partial x, \partial\bar{h}/\partial y)$. According to (17-10a) and (17-10b), this flow must be geostrophic, and according to (17-10c), it must be aligned with the direction of constant layer thickness:

$$-f\bar{v} = -\frac{1}{\rho_0}\frac{\partial \bar{p}}{\partial x}, \tag{17-11a}$$

$$+f\bar{u} = -\frac{1}{\rho_0}\frac{\partial \bar{p}}{\partial y}, \tag{17-11b}$$

$$\bar{u}\frac{\partial \bar{h}}{\partial x} + \bar{v}\frac{\partial \bar{h}}{\partial y} = 0. \tag{17-11c}$$

A thickness gradient is retained because, in some instances, a thermal wind in layers above or below may be accompanied by such a thickness variation. Also, if the vortex lies in the lowest layer, the thickness gradient may represent a bottom slope. The assumption of uniformity of $\bar{u}$, $\bar{v}$, and of the derivatives of $\bar{p}$ and $\bar{h}$ is justified if the ambient-flow properties vary over horizontal distances much larger than the vortex diameter. Defining the velocity components, pressure, and layer-thickness variations proper to the vortex as $u' = u - \bar{u}$, $v' = v - \bar{v}$, $p' = p - \bar{p}$, and $h' = h - \bar{h}$, we can transform equations (17-10) as follows:

$$\frac{\partial u'}{\partial t} + (\bar{u} + u')\frac{\partial u'}{\partial x} + (\bar{v} + v')\frac{\partial u'}{\partial y} - f v' = -\frac{1}{\rho_0}\frac{\partial p'}{\partial x} \tag{17-12a}$$

$$\frac{\partial v'}{\partial t} + (\bar{u} + u')\frac{\partial v'}{\partial x} + (\bar{v} + v')\frac{\partial v'}{\partial y} + f u' = -\frac{1}{\rho_0}\frac{\partial p'}{\partial y} \tag{17-12b}$$

$$\frac{\partial h'}{\partial t} + \bar{u}\frac{\partial h'}{\partial x} + \bar{v}\frac{\partial h'}{\partial y} + \frac{\partial}{\partial x}[(\bar{h} + h')u'] + \frac{\partial}{\partial y}[(\bar{h} + h')v'] = 0. \tag{17-12c}$$

We then define the anomalous layer volume due to the vortex:

$$V = \int\int h' dx\, dy, \tag{17-13}$$

where the integration covers the entire horizontal extent of the layer. The perturbation h' induced by the vortex is assumed to be sufficiently localized to make the preceding integral finite. The use of continuity equation (17-12c) followed by several integrations by parts shows that the temporal derivative of this volume,

$$\frac{dV}{dt} = \int\int \frac{\partial h'}{\partial t}\, dx\, dy,$$

vanishes, as we expect. Defining the coordinates of the vortex position by the volume-weighted averages

$$X = \frac{1}{V}\int\int xh'\, dx\, dy, \quad Y = \frac{1}{V}\int\int yh'\, dx\, dy, \tag{17-14}$$

we can track the vortex displacements by calculating their temporal derivatives. For X, we obtain successively

$$\frac{dX}{dt} = \frac{1}{V}\int\int x\,\frac{\partial h'}{\partial t}\,dx\,dy$$

$$= \frac{-1}{V}\int\int\left\{x\bar{u}\,\frac{\partial h'}{\partial x} + x\bar{v}\,\frac{\partial h'}{\partial y} + x\,\frac{\partial}{\partial x}\,[(\bar{h}+h')u'] + x\,\frac{\partial}{\partial y}\,[(\bar{h}+h')v']\right\}dx\,dy$$

$$= \frac{+1}{V}\int\int[\bar{u}h' + (\bar{h}+h')u']\,dx\,dy$$

$$= \bar{u} + \frac{1}{V}\int\int hu'\,dx\,dy. \tag{17-15a}$$

Similarly, we obtain for the other coordinate

$$\frac{dY}{dt} = \bar{v} + \frac{1}{V}\int\int hv'\,dx\,dy. \tag{17-15b}$$

The preceding integrals cannot be evaluated without knowing with precision the flow field of the vortex. However, a second time derivative will bring forth the acceleration ($\partial u'/\partial t$, $\partial v'/\partial t$), which is provided by the equations of motion, (17-12a) and (17-12b). For the X-coordinate, we obtain

$$\frac{d^2X}{dt^2} = \frac{1}{V}\int\int\left[\frac{\partial h'}{\partial t}\,u' + (\bar{h}+h')\,\frac{\partial u'}{\partial t}\right]dx\,dy$$

$$= \frac{-1}{V}\int\int\left[\frac{\partial}{\partial x}\,(huu') + \frac{\partial}{\partial y}\,(hvu')\right]dx\,dy + \frac{f}{V}\int\int hv'\,dx\,dy - \frac{1}{\rho_0 V}\int\int h\,\frac{\partial p'}{\partial x}\,dx\,dy. \tag{17-16}$$

The pressure anomaly p' associated with the vortex motions can be related by hydrostatic balance to the layer-thickness anomaly:

$$p' = \rho_0 g' h', \tag{17-17}$$

with a suitable definition of the reduced gravity g'. Note that if the vortex is contained in the lowest layer above an uneven bottom, the bottom elevation does not enter (17-17) but instead enters the corresponding hydrostatic balance for the mean-flow properties.

Noting that the first integral in (17-16) vanishes because u' and v' go to zero at large distances from the vortex, that the second integral can be eliminated by use of (17-15b), and that the third integral can be simplified with use of (17-17), we obtain

$$\frac{d^2X}{dt^2} = f\,\frac{dY}{dt} - f\bar{v} + g'\,\frac{\partial \bar{h}}{\partial x}. \tag{17-18a}$$

A similar treatment of the second derivative of Y yields

$$\frac{d^2Y}{dt^2} = -f\frac{dX}{dt} + f\bar{u} + g'\frac{\partial \bar{h}}{\partial y}. \tag{17-18b}$$

Because the gradient of $\bar{h}$ is assumed uniform and f, $\bar{u}$, and $\bar{v}$ are constants, the preceding two equations can be solved for the velocity of the vortex:

$$\frac{dX}{dt} = \left(\bar{u} + \frac{g'}{f}\frac{\partial \bar{h}}{\partial y}\right)(1 - \cos ft) - \left(\bar{v} - \frac{g'}{f}\frac{\partial \bar{h}}{\partial x}\right)\sin ft \tag{17-19a}$$

$$\frac{dY}{dt} = \left(\bar{v} - \frac{g'}{f}\frac{\partial \bar{h}}{\partial x}\right)(1 - \cos ft) + \left(\bar{u} + \frac{g'}{f}\frac{\partial \bar{h}}{\partial y}\right)\sin ft, \tag{17-19b}$$

where the constants of integration have been determined under the assumption that the vortex is not translating initially. In the preceding solution, we recognize inertial oscillations superimposed on a mean drift. This mean drift has two components:

$$c_x = \bar{u} + \frac{g'}{f}\frac{\partial \bar{h}}{\partial y}, \quad c_y = \bar{v} - \frac{g'}{f}\frac{\partial \bar{h}}{\partial x}. \tag{17-20}$$

The first contribution $(\bar{u}, \bar{v})$ indicates that the vortex is entrained by the ambient motions of its containing layer. Together, this entrainment and the inertial oscillations do not distinguish the vortex from a single fluid parcel. The cause of the second contribution, proportional to the gradient of $\bar{h}$, is less obvious and is what really distinguishes a vortex from a fluid parcel.

The existence of a thickness gradient in the vicinity of the vortex implies a nonuniform distribution of potential vorticity, which the swirling motion of the vortex redistributes; fluid parcels on the edge of the vortex are thus stretched and squeezed and develop vorticity anomalies that, in turn, act to displace the main part of the vortex. As the example in Figure 17-9 illustrates, a northward decrease of layer thickness in

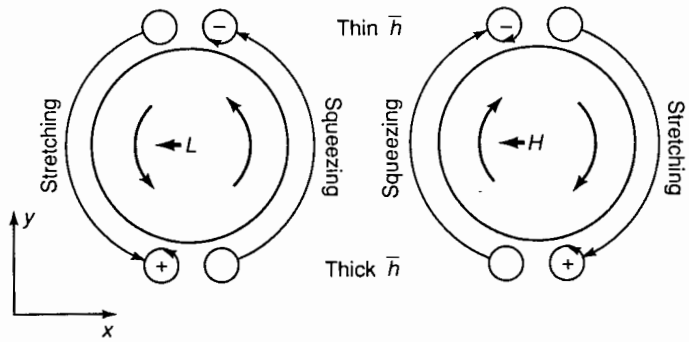

Figure 17-9 Lateral drift of a vortex embedded in layer of varying thickness. The advection of surrounding fluid induces cyclonic and anticyclonic vorticities, which combine to induce a drift of the vortex structure along lines of constant thickness. In the Northern Hemisphere (as drawn in the figure), the vortex moves with the thin-layer side on its right; the direction is opposite in the Southern Hemisphere.

the Northern Hemisphere causes squeezing on parcels moved northward and stretching on those moved southward. (The sense of rotation in the vortex is irrelevant here.) This causes the fluid on the northern flank of the vortex to acquire anticyclonic vorticity and that on the southern flank to acquire cyclonic vorticity. Both vorticity anomalies induce a westward displacement of the bulk of the vortex. Equations (17-20) confirm that those conditions ($\partial \bar{h}/\partial x = 0$, $\partial \bar{h}/\partial y < 0$, $f > 0$) imply a negative c_x and a zero c_y. The general rule is that the vortex translates with the thin-layer side on its right in the Northern Hemisphere and on its left in the Southern Hemisphere.

Gradients in the vortex-containing layer can be caused by one of two reasons. If other layers, above or below, flow at speeds different from that of the vortex layer, there exists a thermal wind, which by virtue of the Margules relation [see (13-5)] requires sloping density surfaces and, therefore, varying layer thicknesses. It is left to the reader to show that in such a case the vorticity-induction mechanism described in the preceding paragraph amounts to a drift of the vortex in the same direction as the thermal wind. The other reason for layer-thickness variations is bottom topography. If the vortex is contained in the lower layer, bounded below by a sloping bottom, fluid parcels surrounding the vortex will be moved up or down this slope and undergo vorticity adjustments. The result (see Figure 17-9 again) is a drift of the vortex with the shallower region to its right in the Northern Hemisphere and to its left in the Southern Hemisphere. Nof (1983) discusses this effect for cold eddy lenses on the ocean bottom.

Note that if the vortex starts from a resting position, its migration is not immediately transverse to the thickness gradient but is up-gradient, as solution (17-19) indicates for small values of time. In the case of a sloping bottom, this implies that the vortex first goes downhill, gradually acquiring a velocity in that direction, and under the action of the Coriolis force has its trajectory subsequently deflected in the direction transverse to the topographic gradient. (Compare this situation to that of Problem 2-6.)

Because of the analogy between a topographic slope and the beta effect (see Section 6-6), the preceding conclusions can be extrapolated to the motion of vortices on the beta-plane. Regardless of their polarity (cyclonic or anticyclonic), vortices have a self-induced westward tendency. Repeating the argument made with Figure 17-9, with the replacement of the thick-to-thin direction by the northward direction, we conclude that surrounding parcels entrained from the southern tip to the northern end acquire planetary vorticity and thus develop anticyclonic relative vorticity. Similarly, the surrounding parcels entrained from north to south develop cyclonic relative vorticity. The combined effect at the latitude of the vortex center is a westward drift. Theories (Cushman-Roisin et al., 1990, and references therein) show that the induced speed is on the order of $\beta_0 R^2$, where R is the internal radius of deformation, being slightly larger for anticyclones than cyclones. However, in both atmosphere and oceans this speed is usually too weak to be noticeable compared to the entrainment by the ambient flow.

Implicit in the preceding derivations was the assumption that all variables related to the vortex decay sufficiently fast away from the vortex core to make all integrals finite. However, in the presence of a potential-vorticity gradient such as one created by a layer-thickness gradient (see the preceding text) or by the beta effect ($\beta_0 = df/dy$), waves are possible (Sections 6-4 and 6-5) and energy can be radiated away to large

distances from the vortex, yielding nonnegligible eddy-related motions there. As it turns out, it is possible to predict, at least qualitatively, the effect of such waves by considering the early time evolution of the vortex. Figure 17-10 depicts the relative-vorticity adjustments brought to surrounding fluid parcels as they are moved by the vortex for

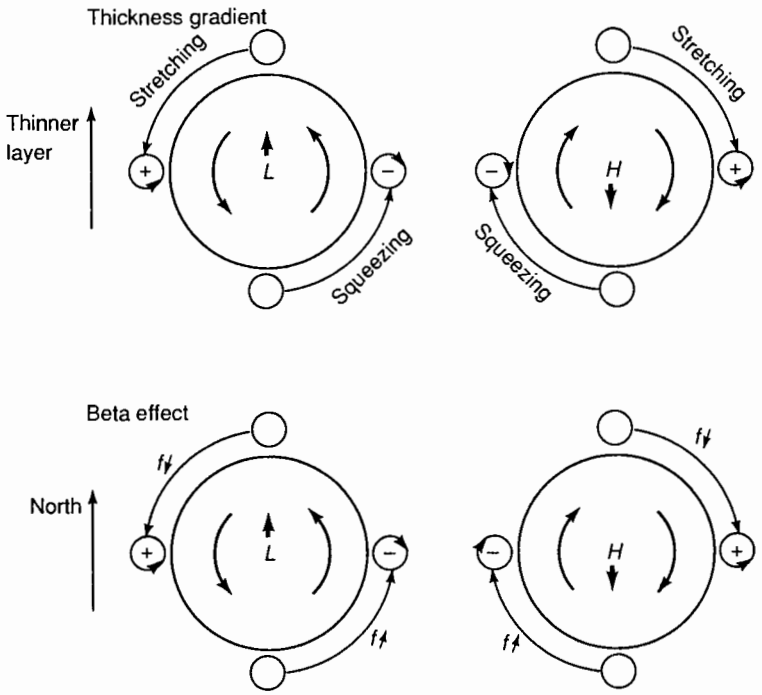

Figure 17-10 Secondary drift of vortices. The advection of surrounding fluid induces cyclonic and anticyclonic vorticities on the flanks of the vortex, which combine to cause a drift as indicated. This drift component is perpendicular and in addition to that depicted in Figure 17-9. Again, the figure is drawn for the Northern Hemisphere; in the Southern Hemisphere, cyclones still move in the direction of smaller layer thickness or poleward, and anticyclones move in the direction of greater layer thickness, or equatorward.

the first quarter of their evolution. As for linear waves (Section 6-6), there is a direct analogy between the layer-thickness gradient and the beta effect: The thin-layer side and the poleward direction are dynamically similar, for they both point to an increase in potential vorticity. After a quarter turn, parcels surrounding the vortex acquire relative vorticity by stretching (or squeezing) or a decrease (or increase) in planetary vorticity. As Figure 17-10 reveals, the cumulative effect in the Northern Hemisphere is a migration of cyclones toward decreasing layer thicknesses or northward; anticyclones migrate in the opposite direction. As vortices move in those directions, their own core fluid undergoes similar stretching or squeezing or planetary-vorticity changes. In all cases,

the net result is a decrease in the absolute value of the relative vorticity and thus an overall spin-down of the vortex.

In the study of hurricane motion, Shapiro (1992) distinctly shows how the trajectory of the hurricane center (a low-pressure center and thus a cyclone) can be explained by the mechanisms just summarized. Here, the beta effect is relatively unimportant, but the presence of a westerly wind aloft and its accompanying layer-thickness gradient (thicker southward) combine to make the hurricane progress in the southeastward direction.

A discussion of geophysical vortices ought to address additional aspects such as axisymmetrization (assuming a nearly circular shape despite anisotropic birthing conditions), instabilities, secondary motions, frictional spin-down, wave radiation, and so on. Partly, because space does not permit a deeper discussion here but mostly because these aspects tend to be quite different in the atmosphere and ocean, the reader interested in atmospheric vortices is referred to the monograph by Anthes (1982), and the reader interested in oceanic vortices is referred to the book edited by Robinson (1983). Laboratory simulations of geophysical vortices have also been conducted; an interesting article on vortex instabilities is that by Griffiths and Linden (1981).

17-3 GEOSTROPHIC TURBULENCE

We alluded to this topic, the study of a large number of interacting vortices, at the end of Chapter 15 when we introduced nonlinear effects in quasi-geostrophic dynamics. Here, we shall tackle the subject from the vortex point of view, without making the quasi-geostrophic assumption.

When several eddies are present and are not too distant from one another, interactions are inevitable. Vortices shear and peel off the sides of their neighbors and, at times, merge to create larger vortices. The sheared elements either curl onto themselves, forming new, smaller vortices, or dissipate under the action of viscosity. The net result is a combination of consolidation and destruction. When many vortices are simultaneously present, the situation is best described in a statistical sense.

A number of important properties can be derived rather simply by considering three integrals of motion, namely, the kinetic energy, the available potential energy, and the *enstrophy*, the latter being the integrated squared vorticity. We thus define the following:

Kinetic energy:
$$KE = \frac{1}{2}\,\rho_0 \int\int\int (u^2 + v^2)\; dx\; dy\; dz, \qquad (17\text{-}21)$$

Available potential energy:
$$APE = \frac{1}{2} \int\int\int N^2 h^2\; dx\; dy\; dz, \qquad (17\text{-}22)$$

Enstrophy:
$$S = \frac{1}{2} \int\int\int \left(\frac{\partial v}{\partial x} - \frac{\partial u}{\partial y}\right)^2 dx\; dy\; dz. \qquad (17\text{-}23)$$

In the formulation of the kinetic energy, the contribution of vertical velocity is usually insignificant. (It is insignificant whenever hydrostatic balance holds.) If the horizontal velocity scale is U, the domain depth is H, and the horizontal area is A, the size of KE is about $\rho_0 U^2 HA$. The definition of the available potential energy was established in (15-29). If the vertical displacements of the density surfaces scale as ΔH ($\Delta H \leq H$, naturally) and if reduced gravity is introduced via $g' = N^2 H$ [see (17-1)], the available potential energy is on the order of $\rho_0 g' \Delta H^2 A$. If the average size of the eddies in the turbulent flow is L, vorticity scales as U/L and enstrophy, as $(U/L)^2 HA$. Finally, if we invoke geostrophy to set the velocity scale, we state $f_0 U \sim g' \Delta H/L$ (barring a substantial barotropic component) and write

$$KE \sim \rho_0 \left(\frac{g' \Delta H}{f_0 \ L} \right)^2 HA, \tag{17-24}$$

$$APE \sim \rho_0 g' \Delta H^2 A, \tag{17-25}$$

$$S \sim \left(\frac{g' \Delta H}{f_0 \ L^2} \right)^2 HA. \tag{17-26}$$

The ratio of kinetic to potential energy is

$$\frac{KE}{APE} \sim \frac{g' H}{f_0^2 L^2} = \left(\frac{R}{L} \right)^2, \tag{17-27}$$

where R is the internal radius of deformation.

As the interactions among vortices proceed, the shearing and tearing of vortices introduce motions at ever shorter scales, until frictional dissipation becomes important. Because S increases much faster than KE with decreasing length scales, while APE is unaffected, friction removes disproportionally more enstrophy than kinetic energy and, surely, potential energy. In first approximation, we can assume that the total energy is conserved, while enstrophy decays with time. In a fixed domain (HA = constant) and with constant f_0 and g' values (no heating or cooling), a decrease in enstrophy requires, by virtue of (17-26), a decrease in the ratio $\Delta H/L^2$.

At short length scales ($L \ll R$), the energy consists primarily of kinetic energy, via (17-27), and its near conservation requires that $\Delta H/L$ remain approximately constant. The only possibility that satisfies both requirements is a steady increase of the length scale L, with a proportional increase in eddy amplitude ΔH. Thus, the vortices become, on average, larger and stronger. Obviously, to conserve the total space allowed to them, they also become fewer. There is thus a natural tendency toward successive eddy mergers. With every merger, energy is consolidated into larger structures with concomitant enstrophy losses.

As the length scale increases toward the radius of deformation, the relative importance of potential energy increases. Because APE increases like ΔH^2, further increases in mean eddy amplitude ΔH require corresponding decreases in kinetic energy, to preserve the total energy, and $\Delta H^2/L^2$ must begin to decrease. The result is that ΔH and L continue to increase but no longer proportionally, L increasing faster than ΔH.

As the length scale continues to increase, indicating continued merging activity, it will eventually become much larger than R. Then, the energy is primarily in the form of potential energy, and its conservation requires a saturated value of ΔH. Further enstrophy decrease under frictional action is possible only with a further increase in length scale L (Rhines, 1975; Salmon, 1982). In sum, the interactions of a larger number of vortices without addition of energy lead to an irreversible tendency toward fewer and larger vortices. This implies an emergence of coherent structures from a random initial vorticity field. As for the mean eddy amplitude, it increases only up to a certain point. The maximum possible eddy amplitude is achieved when almost all the energy available is in the form of available potential energy—that is,

$$\Delta H_{\max} \sim \sqrt{\frac{E}{\rho_0 g' A}}, \tag{17-28}$$

where E is the total energy present in the system ($E = KE + APE$) and A is the horizontal area of the system. Should this value exceed the depth H of the domain, vortex amplitudes will be limited by the latter and not all the energy can be turned into potential energy; a certain portion of the energy must remain in the form of kinetic energy, implying a limit to the length scale L.

At the time of this writing, geostrophic turbulence is a topic of great interest. New results are published at a rapid pace, and it is not appropriate within the context of the present volume to attempt to summarize them. Recent results concerning the emergence of coherent vortices in quasi-geostrophic turbulence can be found in McWilliams (1984; 1989). Let us also note that the tendency toward successive merger is at the basis of the contemporary theories (Williams and Wilson, 1988, and references therein) that explain the persistence of the Great Red Spot in the atmosphere of the planet Jupiter (Figure 1-4). Finally, the question arises as to why no single dominating vortex occurs in our atmosphere as on Jupiter. The answer lies in diabatic and orographic effects constantly acting to form and destroy existing atmospheric vortices. In other words, geostrophic turbulence in the earth's atmosphere is never freely evolving for very long. Similarly, wind forcing over the ocean and dissipation by internal waves and in coastal areas combine to prevent oceanic geostrophic turbulence from following its intrinsic evolution.

PROBLEMS

17-1. Consider the center fluid parcel ($y = 0$) of the Gaussian jet $u(y) = U \exp(-y^2/2L^2)$ with $U = 10$ m/s and $L = 100$ km. On the f-plane, what is the shear vorticity acquired by that parcel in a rightward meander of curvature $K = 1/800$ km? On the beta plane, what meridional displacement Y would permit the parcel to conserve its speed and maintain its center position?

17-2. For the one-layer reduced gravity model (12-34) through (12-36), express the gradient-wind balance for steady circular vortices on the f-plane. If the layer thickness is H at the

center and the density interface outcrops at radius a [i.e., $h(r = 0) = H$, $h(r = a) = 0$], show that H and a must satisfy the inequality

$$a \geq \frac{\sqrt{8g'H}}{f}.$$

17-3. Take a stretch of the jet profile $u(y) = U(1 - |y|/a)$ in $|y| \leq a$, $u(y) = 0$ elsewhere (see Figure 7-4), and bend it to create a clockwise vortex. On the f-plane and in the absence of vertical variations, what is the orbital-velocity profile that preserves vorticity? How does the pressure anomaly in the vortex compare to the pressure difference across the jet? Finally, show that the proportion of fluids with each vorticity is the same in the vortex as in the straight jet.

17-4. Determine the behavior of an eastward jet in the Northern Hemisphere flowing over a topographic step-up followed by a step-down of equal height. Is the flow oscillatory beyond the second step? Also discuss the cases where the distance between the two steps is short and long compared to the critical meander scale.

17-5. Redo Problem 17-4 for a westward jet in the Southern Hemisphere.

17-6. Hurricane Hugo (10–22 September 1989 in the western North Atlantic; see Figure 1-1) had a maximum wind speed of 62 m/s and a low central pressure of 941.4 millibars during its passage over Guadeloupe on 17 September (Case and Mayfield, 1990). Assuming that the normal pressure outside the hurricane was 1010 millibars, estimate the storm's radius and importance of the centrifugal force relative to the Coriolis force (latitude = 16°N).

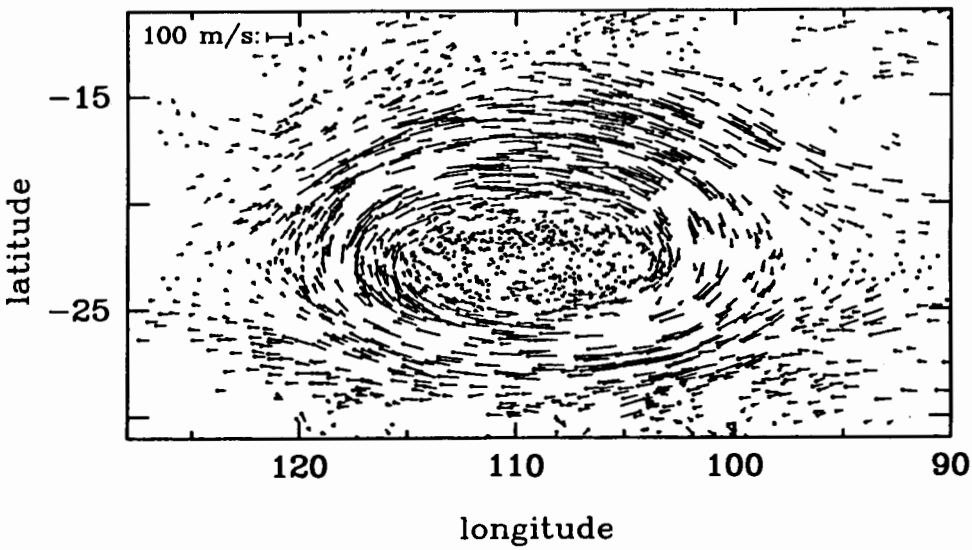

Figure 17-11 Velocity field on Jupiter in and around the Great Red Spot, obtained after tracking small cloud features in sequential images from *Voyager* spacecraft (Problem 17-8). The origin of each vector is indicated by a dot. (From Dowling and Ingersoll, 1988.)

17-7. Using the gradient-wind balance (17-8) in a reduced-gravity model ($p = \rho g' h$), explore lenslike vortex solutions where the interface exhibits a paraboloical shape between a central maximum depth ($h = H$ at $r = 0$) and a peripheral outcrop ($h = 0$ at $r = R$). Show that the flow is in solid-body rotation. Relate vortex radius R to central depth H and discuss the limiting cases of wide/shallow and narrow/deep vortices. Do you recover an inequality of type (17-9)?

17-8. In first approximation, the thick atmosphere of Jupiter can be modeled as a reduced-gravity system with $g' = 2.64$ m/s^2. Knowing that planet radius is 69,000 km and that one Jovian day is only 10 earth-hours long, derive the thickness h of moving fluid for a few radial sections across the wind-velocity chart provided in Figure 17-11.

SUGGESTED LABORATORY DEMONSTRATION

In addition to the demonstration outlined at the end of the previous chapter (illustrating well the concepts of jets and vortices) and to the traditional hurricane demonstration (described in most English-language encyclopedias), the following is also suggested.

Equipment

Rotating tank, dyed ice disk.

Experiment

Fill the tank with water at room temperature and spin. Once the fluid has achieved solid-body rotation, carefully deposit the ice disk on the surface. Observe the development of vortices where cold, dyed water from the melting ice sinks and stretches vertically. Do all vortices rotate in the same direction? Why?

Melvin Ernest Stern

1929 –

Melvin Stern has been an important contributor to the GFD Summer Program at the Woods Hole Oceanographic Institution (see the end of Chapter 1) and has had a major influence on the evolution of the field since then. His early work in meteorology was followed by fundamental contributions to our understanding of baroclinic instability (work with J. G. Charney) and of salt fingering (an oceanic small-scale diffusive process). After publishing the book *Ocean Circulation Physics* (Academic Press, 1975), Stern dedicated an increasing amount of time and effort to the investigation of vortices (he discovered the *modon* solution; see Section 15-6), jets, and jet-vortex interactions, complementing his theoretical studies with original and illuminating laboratory experiments. (*Photo by the author.*)

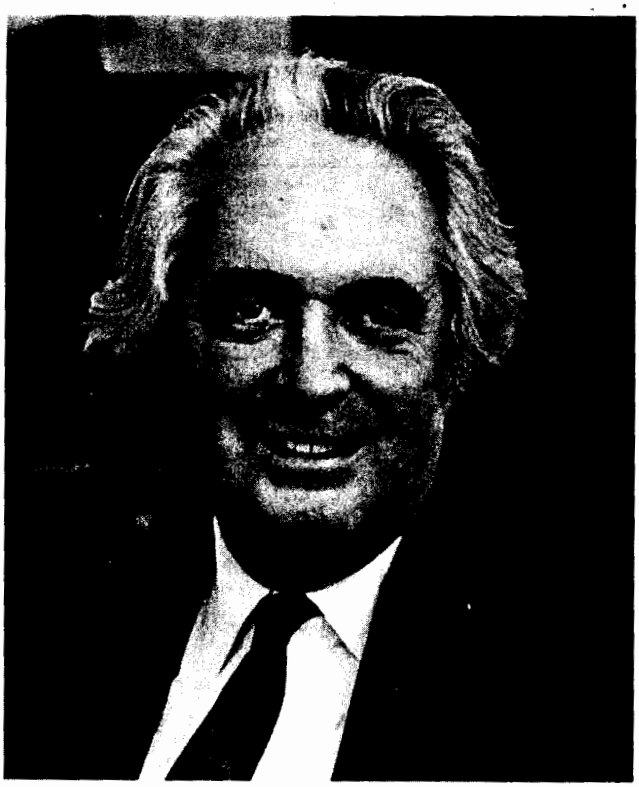

Allan Richard Robinson

1932 –

An avowed "phenomenologist," Allan Richard Robinson is counted among the founding fathers of geophysical fluid dynamics because of his seminal contributions on the dynamics of rotating and stratified fluids, boundary-layer flows, continental shelf waves, and the maintenance of the oceanic thermocline. During the 1970s, he chaired and co-chaired a series of international programs that established the existence and importance of intermediate-scale eddies in the open ocean, the *internal weather of the sea*. His research has led him to formulate numerical models for ocean forecasting (e.g., Gulf Stream meandering) and to emphasize the role of ocean physics in regulating biological activity. Robinson has also contributed significantly to the development of techniques for the assimilation of data in ocean-forecasting models. Underlying his accomplishments is the firm belief that "curiosity about nature is the primary driving force and rationalization for research." (*Photo credit: A. R. Robinson.*)